

A STABLE NUMERICAL ALGORITHM FOR THE BRINKMAN EQUATIONS BY WEAK GALERKIN FINITE ELEMENT METHODS

LIN MU*, JUNPING WANG[†], AND XIU YE[‡]

Abstract. This paper presents a stable numerical algorithm for the Brinkman equations by using weak Galerkin (WG) finite element methods. The Brinkman equations can be viewed mathematically as a combination of the Stokes and Darcy equations which model fluid flow in a multi-physics environment, such as flow in complex porous media with a permeability coefficient highly varying in the simulation domain. In such applications, the flow is dominated by Darcy in some regions and by Stokes in others. It is well known that the usual Stokes stable elements do not work well for Darcy flow and vice versa. The challenge of this study is on the design of numerical schemes which are stable for both the Stokes and the Darcy equations. This paper shows that the WG finite element method is capable of meeting this challenge by providing a numerical scheme that is stable and accurate for both Darcy and the Stokes dominated flows. Error estimates of optimal order are established for the corresponding WG finite element solutions. The paper also presents some numerical experiments that demonstrate the robustness, reliability, flexibility and accuracy of the WG method for the Brinkman equations.

Key words. Weak Galerkin, finite element methods, the Brinkman equations, polyhedral meshes.

AMS subject classifications. Primary, 65N15, 65N30, 76D07; Secondary, 35B45, 35J50

1. Introduction. This paper is concerned with the development of stable numerical methods for the Brinkman equations by using weak Galerkin finite element methods. The Brinkman equations model fluid flow in complex porous media with a permeability coefficient highly varying so that the flow is dominated by Darcy in some regions and by Stokes in others. In a simple form, the Brinkman model seeks unknown functions u and p satisfying

$$(1.1) \quad -\mu\Delta\mathbf{u} + \nabla p + \mu\kappa^{-1}\mathbf{u} = \mathbf{f} \quad \text{in } \Omega,$$

$$(1.2) \quad \nabla \cdot \mathbf{u} = 0 \quad \text{in } \Omega,$$

$$(1.3) \quad \mathbf{u} = \mathbf{g}, \quad \text{on } \partial\Omega,$$

where μ is the fluid viscosity and κ denotes the permeability tensor of the porous media which occupies a polygonal or polyhedral domain Ω in \mathbb{R}^d ($d = 2, 3$). u and p represent the velocity and the pressure of the fluid, and f is a momentum source term. For simplicity, we consider (1.1) and (1.2) with $\mathbf{g} = 0$ and $\mu = 1$ (note that one can always scale the solution with μ).

Assume that there exist two positive numbers $\lambda_1, \lambda_2 > 0$ such that

$$(1.4) \quad \lambda_1 \xi^t \xi \leq \xi^t \kappa^{-1} \xi \leq \lambda_2 \xi^t \xi, \quad \forall \xi \in \mathbb{R}^d.$$

*Department of Mathematics, Michigan State University, East Lansing, MI 48824 (linmu@msu.edu)

[†]Division of Mathematical Sciences, National Science Foundation, Arlington, VA 22230 (jwang@nsf.gov). The research of Wang was supported by the NSF IR/D program, while working at the Foundation. However, any opinion, finding, and conclusions or recommendations expressed in this material are those of the author and do not necessarily reflect the views of the National Science Foundation.

[‡]Department of Mathematics, University of Arkansas at Little Rock, Little Rock, AR 72204 (xxye@ualr.edu). This research was supported in part by National Science Foundation Grant DMS-1115097

Here ξ is understood as a column vector and ξ^t is the transpose of ξ . We consider the case where λ_1 is of unit size and λ_2 is possibly of large size.

The Brinkman equations (1.1) and (1.2) are used to model fluid motion in porous media with fractures. The model can also be regarded as a generalization of the Stokes equations that represent a valid approximation of the Navier-Stokes equations at low Reynolds numbers. Modeling fluid flow in complex media with multiphysics has significant impact for many industrial and environmental problems such as industrial filters, open foams, or natural vuggy reservoirs. The permeability with high contrast determines that flow velocity may vary greatly through porous media. Mathematically, the Brinkman equations can be viewed as a combination of the Stokes and the Darcy equations, but with change of type from place to place in the computational domain. Due to the type change, numerical schemes for the Brinkman equations must be carefully designed to accommodate both the Stokes and Darcy simultaneously. The numerical experiments in [12] indicate that the convergent rate deteriorates as the Brinkman becomes Darcy-dominating when certain stable Stokes elements are used; such elements include the conforming P_2 - P_0 element, the nonconforming Crouzeix-Raviart element, and the Mini element. Similarly, the convergent rate deteriorates as the Brinkman is Stokes-dominating when Darcy stable elements such as the lowest order RaviartThomas element [12] are used.

The main challenge for solving Brinkman equations is in the construction of numerical schemes that are stable for both the Darcy and the Stokes equations. In literature, a great deal of effort has been made in meeting this challenge by modifying either existing Stokes elements or Darcy elements to obtain new Brinkman stable elements. For example, methods based on Stokes elements have been studied in [1] and methods based on Darcy elements can be found in [11, 12].

Weak Galerkin (WG) is a general finite element technique for partial differential equations in which differential operators are approximated by their weak forms as distributions. WG methods, by design, make use of discontinuous piecewise polynomials on finite element partitions with arbitrary shape of polygons and polyhedrons. The flexibility of WG on the selection of approximating polynomials makes it an excellent candidate for providing stable numerical schemes for PDEs with multi-physics properties. The weak Galerkin method was first introduced in [13, 14] for the second order elliptic problem.

The goal of this paper is to develop a stable weak Galerkin finite element method for the Brinkman equations. In Section 2, a WG finite element scheme will be introduced for the Brinkman model. It demonstrates that WG offers a natural and straightforward framework for constructing stable numerical algorithms for the Brinkman equations. In Section 6, an optimal order error estimate shall be established for the velocity and pressure approximations. In Section 7, some numerical experiments are conducted to demonstrate the reliability, flexibility and accuracy of the weak Galerkin method for the Brinkman equations. In particular, the first example, which has known analytical solution, is designed to demonstrate uniform convergence of the WG method with respect to certain parameters. The rest of the examples are relevant to practical problems for which no analytical solutions are known. In addition, flow through different geometries are investigated in the numerical experiments. These geometries include vuggy structure, open foam and fibrous materials. Figure 1 depicts the profile of the permeability inverse for three highly varying porous media under the present study.

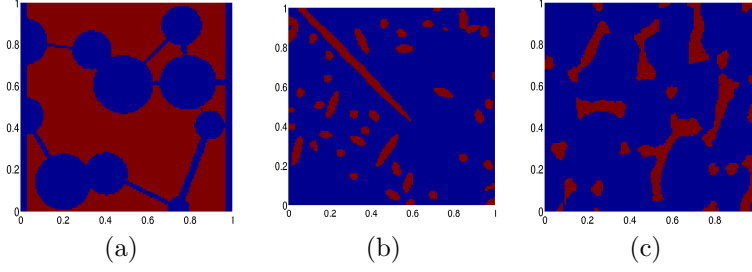


FIG. 1.1. (a) vuggy medium; (b) fibrous material; (c) open foam.

2. A Weak Galerkin Finite Element Method. First, we use the standard definition for the Sobolev space $H^s(D)$ and their associated inner products $(\cdot, \cdot)_{s,D}$, norms $\|\cdot\|_{s,D}$, and seminorms $|\cdot|_{s,D}$ for any $s \geq 0$. We shall drop the subscript D when $D = \Omega$ and s as $s = 0$ in the norm and inner product notation.

Let \mathcal{T}_h be a partition of the domain Ω consisting of polygons in two dimension or polyhedra in three dimension satisfying a set of conditions as specified in [14]. Denote by \mathcal{E}_h the set of all flat faces in \mathcal{T}_h , and let $\mathcal{E}_h^0 = \mathcal{E}_h \setminus \partial\Omega$ be the set of all interior faces.

For $k \geq 1$, we define two weak Galerkin finite element spaces associated with \mathcal{T}_h as follows. For the velocity unknown, we have

$$(2.1) \quad V_h = \{ \mathbf{v} = \{ \mathbf{v}_0, \mathbf{v}_b \} : \{ \mathbf{v}_0, \mathbf{v}_b \}|_T \in [P_k(T)]^d \times [P_k(e)]^d, e \in \partial T, \mathbf{v}_b = 0 \text{ on } \partial\Omega \},$$

and for pressure

$$(2.2) \quad W_h = \{ q \in L_0^2(\Omega) : q|_T \in P_{k-1}(T) \}.$$

By a weak function $\mathbf{v} = \{ \mathbf{v}_0, \mathbf{v}_b \}$ we mean $\mathbf{v} = \mathbf{v}_0$ inside of the element T and $\mathbf{v} = \mathbf{v}_b$ on the boundary of the element T . We would like to emphasize that any function $\mathbf{v} \in V_h$ has a single value v_b on each edge $e \in \mathcal{E}_h$.

Our weak Galerkin finite element method is based on the following variational formulation for (1.1)-(1.3): find $(\mathbf{u}, p) \in [H_0^1(\Omega)]^d \times L_0^2(\Omega)$ satisfying

$$(2.3) \quad (\nabla \mathbf{u}, \nabla \mathbf{v}) + (\kappa^{-1} \mathbf{u}, \mathbf{v}) - (\nabla \cdot \mathbf{v}, p) = (\mathbf{f}, \mathbf{v}),$$

$$(2.4) \quad (\nabla \cdot \mathbf{u}, q) = 0$$

for all $(\mathbf{v}, q) \in [H_0^1(\Omega)]^d \times L_0^2(\Omega)$.

The key in the design of WG finite element scheme is the use of weak derivatives in the place of strong derivatives in the variational form for the underlying partial differential equations. Note that the two differential operators used in (2.3) and (2.4) are the gradient and divergence operators. Weak gradient and weak divergence operators, along with their discrete analogues, have been defined in [13] and [14] respectively. For completeness, we recall the discrete weak divergence and weak gradient operators as follows. For each $\mathbf{v} = \{ \mathbf{v}_0, \mathbf{v}_b \} \in V_h$, the discrete weak divergence $\nabla_{w,k-1} \cdot \mathbf{v} \in P_{k-1}(T)$ is given on each element T such that

$$(2.5) \quad (\nabla_{w,k-1} \cdot \mathbf{v}, q)_T = -(\mathbf{v}_0, \nabla q)_T + \langle \mathbf{v}_b, q \mathbf{n} \rangle_{\partial T}, \quad \forall q \in P_{k-1}(T).$$

Similarly, the discrete weak gradient $\nabla_{w,k-1} \mathbf{v} \in P_{k-1}(T)^{d \times d}$ is defined on each element T by

$$(2.6) \quad (\nabla_{w,k-1} \mathbf{v}, \tau)_T = -(\mathbf{v}_0, \nabla \cdot \tau)_T + \langle \mathbf{v}_b, \tau \cdot \mathbf{n} \rangle_{\partial T}, \quad \forall \tau \in [P_{k-1}(T)]^{d \times d}.$$

Without confusion, we will drop the subscript $k-1$ and use $\nabla_w \cdot$ and ∇_w to denote $\nabla_{w,k-1} \cdot$ and $\nabla_{w,k-1}$. We will also use $(\nabla_w \cdot \mathbf{v}, q)$ and $(\nabla_w \mathbf{v}, \nabla_w \mathbf{w})$ to denote $\sum_{T \in \mathcal{T}_h} (\nabla_w \cdot \mathbf{v}, q)_T$ and $\sum_{T \in \mathcal{T}_h} (\nabla_w \mathbf{v}, \nabla_w \mathbf{w})_T$ respectively.

We are now in a position to describe a weak Galerkin finite element method for the Brinkman equations (1.1)-(1.3). To this end, we introduce three bilinear forms as follows

$$\begin{aligned} s(\mathbf{v}, \mathbf{w}) &= \sum_{T \in \mathcal{T}_h} h_T^{-1} \langle \mathbf{v}_0 - \mathbf{v}_b, \mathbf{w}_0 - \mathbf{w}_b \rangle_{\partial T}, \\ a(\mathbf{v}, \mathbf{w}) &= (\nabla_w \mathbf{v}, \nabla_w \mathbf{w}) + (\kappa^{-1} \mathbf{v}_0, \mathbf{w}_0) + s(\mathbf{v}, \mathbf{w}), \\ b(\mathbf{v}, q) &= (\nabla_w \cdot \mathbf{v}, q). \end{aligned}$$

WEAK GALERKIN ALGORITHM 1. Find $\mathbf{u}_h = \{\mathbf{u}_0, \mathbf{u}_b\} \in V_h$ and $p_h \in W_h$ such that

$$(2.7) \quad a(\mathbf{u}_h, \mathbf{v}) - b(\mathbf{v}, p_h) = (f, \mathbf{v}_0), \quad \forall \mathbf{v} = \{\mathbf{v}_0, \mathbf{v}_b\} \in V_h$$

$$(2.8) \quad b(\mathbf{u}_h, q) = 0, \quad \forall q \in W_h.$$

The corresponding solution $(\mathbf{u}_h; p_h)$ is called *WG finite element solution* for (1.1)-(1.3).

3. Existence and Uniqueness. The WG finite element scheme (2.7)-(2.8) is a saddle-point problem. However, the theory of Babuška [2] and Brezzi [4] is hard to apply directly due to the large variation of the permeability tensor. But the main ideas of Babuška and Brezzi are still applicable.

For the velocity space V_h , we use a norm $\|\cdot\|$ induced by the symmetric and positive bilinear form $a(\cdot, \cdot)$ defined as follows

$$(3.1) \quad \|\mathbf{v}\|^2 = a(\mathbf{v}, \mathbf{v}) = \|\kappa^{-\frac{1}{2}} \mathbf{v}_0\|^2 + \|\nabla_w \mathbf{v}\|^2 + \sum_{T \in \mathcal{T}_h} h_T^{-1} \|\mathbf{v}_0 - \mathbf{v}_b\|_{\partial T}^2.$$

For convenience, we introduce another norm $\|\cdot\|_{1,h}$ in V_h

$$(3.2) \quad \|\mathbf{v}\|_{1,h}^2 = \|\nabla_w \mathbf{v}\|^2 + \sum_{T \in \mathcal{T}_h} h_T^{-1} \|\mathbf{v}_0 - \mathbf{v}_b\|_{\partial T}^2.$$

It is not hard to see that $\|\cdot\|_{1,h}$ is a discrete H^1 norm for V_h .

For the pressure space W_h , we use the following norm

$$(3.3) \quad |q|_{1,h}^2 = \sum_{T \in \mathcal{T}_h} \|\kappa^{\frac{1}{2}} \nabla q\|_T^2 + h^{-1} \sum_{e \in \mathcal{E}_h^0} \|\llbracket q \rrbracket\|_e^2,$$

where $\llbracket q \rrbracket$ is the jump of the function q on the set of interior edges \mathcal{E}_h^0 .

For simplicity of analysis, the rest of the paper assumes that the permeability tensor κ has constant value on each element $T \in \mathcal{T}_h$. The result can be easily extended to the case of piecewise smooth tensor κ .

The following result is straightforward by using the definition of $\|\cdot\|$ and the usual Cauchy-Schwarz inequality.

LEMMA 3.1. For any $\mathbf{v}, \mathbf{w} \in V_h$, we have the following boundedness and coercivity for the bilinear form $a(\cdot, \cdot)$

$$(3.4) \quad |a(\mathbf{v}, \mathbf{w})| \leq \|\mathbf{v}\| \|\mathbf{w}\|,$$

$$(3.5) \quad a(\mathbf{v}, \mathbf{v}) = \|\mathbf{v}\|^2.$$

For any $\rho \in W_h \subset L_0^2(\Omega)$ and $\mathbf{v} \in V_h$, we have from the definition of the discrete weak divergence that

$$\begin{aligned} b(\mathbf{v}, \rho) &= \sum_{T \in \mathcal{T}_h} (\nabla_w \cdot \mathbf{v}, \rho)_T \\ &= \sum_{T \in \mathcal{T}_h} \{ \langle \mathbf{v}_b, \rho \mathbf{n} \rangle_{\partial T} - (\mathbf{v}_0, \nabla \rho)_T \} \\ &= - \sum_{T \in \mathcal{T}_h} (\mathbf{v}_0, \nabla \rho)_T + \sum_{e \in \mathcal{E}_h^0} \langle \mathbf{v}_b, \llbracket \rho \rrbracket \mathbf{n}_e \rangle_e, \end{aligned}$$

where \mathbf{n}_e is a prescribed normal direction to the edge e , and $\llbracket \rho \rrbracket$ stands for the jump of the function ρ on edge e . In particular, if $\mathbf{v} = \mathbf{v}^* = \{\mathbf{v}_0^*, \mathbf{v}_b^*\}$ is given by

$$(3.6) \quad \mathbf{v}_0^* = -\kappa \nabla \rho, \quad \mathbf{v}_b^* = h^{-1} \llbracket \rho \rrbracket \mathbf{n}_e,$$

then

$$(3.7) \quad b(\mathbf{v}^*, \rho) = \sum_{T \in \mathcal{T}_h} (\kappa \nabla \rho, \nabla \rho)_T + h^{-1} \sum_{e \in \mathcal{E}_h^0} \|\llbracket \rho \rrbracket\|_e^2 = |\rho|_{1,h}^2.$$

Thus, \mathbf{v}^* can be regarded as an artificial flux for the ‘‘pressure’’ function ρ . For convenience, we introduce a notation for this artificial flux:

$$(3.8) \quad F(\rho) := \{-\kappa \nabla \rho, h^{-1} \llbracket \rho \rrbracket \mathbf{n}_e\}.$$

LEMMA 3.2. *For any $\rho \in \mathcal{W}_h$, let $F(\rho)$ be the artificial flux given by (3.8). Then, we have*

$$(3.9) \quad b(F(\rho), \rho) = |\rho|_{1,h}^2.$$

Furthermore, there exists a constant C such that

$$(3.10) \quad \|F(\rho)\|_{1,h} \leq Ch^{-1} |\rho|_{1,h}.$$

Proof. The identity (3.9) is given by (3.7). It remains to derive the estimate (3.10). To this end, write $\{\mathbf{v}_0^*, \mathbf{v}_b^*\} = F(\rho)$. From the definition (3.2), we have

$$(3.11) \quad \|F(\rho)\|_{1,h}^2 = \|\nabla_w \mathbf{v}^*\|^2 + \sum_{T \in \mathcal{T}_h} h_T^{-1} \|\mathbf{v}_0^* - \mathbf{v}_b^*\|_{\partial T}^2.$$

To estimate the first term $\|\nabla_w \mathbf{v}^*\|^2$, we recall from the definition of $\nabla_w \mathbf{v}^*$ that

$$(\nabla_w \mathbf{v}^*, \tau)_T = -(\mathbf{v}_0^*, \nabla \cdot \tau)_T + \langle \mathbf{v}_b^*, \tau \cdot \mathbf{n} \rangle_{\partial T}.$$

Using (3.8) we obtain

$$(\nabla_w \mathbf{v}^*, \tau)_T = (\kappa \nabla \rho, \nabla \cdot \tau)_T + h^{-1} \langle \llbracket \rho \rrbracket \mathbf{n}, \tau \cdot \mathbf{n} \rangle_{\partial T \cap \mathcal{E}_h^0}.$$

The above equation, together with the usual inverse inequality for finite element functions implies

$$\|\nabla_w \mathbf{v}^*\|_T \leq Ch^{-1} \|\kappa \nabla \rho\|_T + Ch^{-\frac{3}{2}} \|\llbracket \rho \rrbracket\|_{\partial T \cap \mathcal{E}_h^0}.$$

Thus, from the assumption (1.4) we have

$$\|\nabla_w \mathbf{v}^*\|_T^2 \leq Ch^{-2} \lambda_1^{-1} \|\kappa^{\frac{1}{2}} \nabla \rho\|_T^2 + Ch^{-3} \|\llbracket \rho \rrbracket\|_{\partial T \cap \mathcal{E}_h^0}^2.$$

Summing over all element $T \in \mathcal{T}_h$ yields

$$\begin{aligned} \|\nabla_w \mathbf{v}^*\|^2 &\leq Ch^{-2} \lambda_1^{-1} \sum_{T \in \mathcal{T}_h} (\kappa \nabla \rho, \nabla \rho)_T + h^{-3} \sum_{e \in \mathcal{E}_h^0} \|\llbracket \rho \rrbracket\|_e^2 \\ (3.12) \quad &\leq Ch^{-2} |\rho|_{1,h}^2, \end{aligned}$$

where we have used the assumption that λ_1 is of unit size. As to the second term on the right-hand side of (3.11), we use (3.8) and the trace inequality (5.4) to obtain

$$\begin{aligned} \|\mathbf{v}_0^* - \mathbf{v}_b^*\|_{\partial T}^2 &\leq 2\|\kappa \nabla \rho\|_{\partial T}^2 + 2h^{-2} \|\llbracket \rho \rrbracket\|_{\partial T \cap \mathcal{E}_h^0}^2 \\ &\leq C(h^{-1} \|\kappa \nabla \rho\|_T^2 + h^{-2} \|\llbracket \rho \rrbracket\|_{\partial T \cap \mathcal{E}_h^0}^2). \end{aligned}$$

Thus, it follows from (1.4) that

$$\begin{aligned} \sum_{T \in \mathcal{T}_h} h_T^{-1} \|\mathbf{v}_0^* - \mathbf{v}_b^*\|_{\partial T}^2 &\leq Ch^{-2} \lambda_1^{-1} \sum_{T \in \mathcal{T}_h} \|\kappa^{\frac{1}{2}} \nabla \rho\|_T^2 + Ch^{-3} \sum_{e \in \mathcal{E}_h^0} \|\llbracket \rho \rrbracket\|_e^2 \\ (3.13) \quad &\leq Ch^{-2} |\rho|_{1,h}^2. \end{aligned}$$

Here we again used the fact that λ_1 is of unit size. Substituting (3.12) and (3.13) into (3.11) yields the desired estimate (3.10). This completes the proof of the lemma. \square

LEMMA 3.3. *The weak Galerkin finite element scheme (2.7)-(2.8) has one and only one solution.*

Proof. Since the number of unknowns is the same as the number of equations, then the solution existence is equivalent to its uniqueness. Thus, it suffices to show that the homogeneous problem (i.e., $f = 0$) has only trivial solutions. To this end, assume that $f = 0$ in (2.7). By letting $\mathbf{v} = \mathbf{u}_h$ in (2.7) and $q = p_h$ in (2.8) we obtain

$$a(\mathbf{u}_h, \mathbf{u}_h) - b(\mathbf{u}_h, p_h) = 0, \quad b(\mathbf{u}_h, p_h) = 0.$$

It follows that

$$\|\mathbf{u}_h\| = \sqrt{a(\mathbf{u}_h, \mathbf{u}_h)} = 0,$$

and hence $u_h = 0$.

To show $p_h = 0$, we use the equation (2.7) and the fact that $f = 0$ and $\mathbf{u}_h = 0$ we obtain

$$b(\mathbf{v}, p_h) = 0.$$

By letting $\mathbf{v} = F(p_h)$ be the artificial flux of p_h , we have from (3.9) that

$$0 = b(F(p_h), p_h) = |p_h|_{1,h}.$$

Thus, $p_h = 0$ and the lemma is completely proved. \square

4. Error Equations. Denote by Q_0 the L^2 projection operator from $[L^2(T)]^d$ onto $[P_k(T)]^d$. For each edge/face $e \in \mathcal{E}_h$, denote by Q_b the L^2 projection from $[L^2(e)]^d$ onto $[P_k(e)]^d$. We shall combine Q_0 with Q_b by writing $Q_h = \{Q_0, Q_b\}$. In addition, let \mathbb{Q}_h and \mathbf{Q}_h be two local L^2 projections onto $P_{k-1}(T)$ and $[P_{k-1}(T)]^{d \times d}$, respectively.

LEMMA 4.1. *The projection operators Q_h , \mathbf{Q}_h , and \mathbb{Q}_h satisfy the following commutative properties*

$$(4.1) \quad \nabla_w(Q_h \mathbf{v}) = \mathbf{Q}_h(\nabla \mathbf{v}), \quad \forall \mathbf{v} \in [H^1(\Omega)]^d,$$

$$(4.2) \quad \nabla_w \cdot (Q_h \mathbf{v}) = \mathbb{Q}_h(\nabla \cdot \mathbf{v}), \quad \forall \mathbf{v} \in H(\text{div}, \Omega).$$

The proof of Lemma 4.1 is straightforward and can be found in [13] and [14].

The following are two useful identities:

$$(4.3) \quad (\nabla_w(Q_h \mathbf{u}), \nabla_w \mathbf{v})_T = (\nabla \mathbf{u}, \nabla \mathbf{v}_0)_T - \langle \mathbf{v}_0 - \mathbf{v}_b, \mathbf{Q}_h(\nabla \mathbf{u}) \cdot \mathbf{n} \rangle_{\partial T}.$$

$$(4.4) \quad (\mathbf{v}_0, \nabla p) = -(\nabla_w \cdot \mathbf{v}, \mathbb{Q}_h p) + \sum_{T \in \mathcal{T}_h} \langle \mathbf{v}_0 - \mathbf{v}_b, (p - \mathbb{Q}_h p) \mathbf{n} \rangle_{\partial T}.$$

Equations (4.3) and (4.4) can be verified easily; they were first derived in [13] and [14], respectively.

Introduce two functionals as follows

$$(4.5) \quad l_1(\mathbf{v}, \mathbf{u}) = \sum_{T \in \mathcal{T}_h} \langle \mathbf{v}_0 - \mathbf{v}_b, \nabla \mathbf{u} \cdot \mathbf{n} - \mathbf{Q}_h(\nabla \mathbf{u}) \cdot \mathbf{n} \rangle_{\partial T},$$

$$(4.6) \quad l_2(\mathbf{v}, p) = \sum_{T \in \mathcal{T}_h} \langle \mathbf{v}_0 - \mathbf{v}_b, (p - \mathbb{Q}_h p) \mathbf{n} \rangle_{\partial T}.$$

LEMMA 4.2. *Let $\mathbf{u}_h = \{\mathbf{u}_0, \mathbf{u}_b\}$ be the WG finite element solution arising from the WEAK GALERKIN ALGORITHM 1. Let $\mathbf{e}_h = \{\mathbf{e}_0, \mathbf{e}_b\} = \{Q_0 \mathbf{u} - \mathbf{u}_0, Q_b \mathbf{u} - \mathbf{u}_b\}$ and $\varepsilon_h = \mathbb{Q}_h p - p_h$ be the error between the WG finite element solution and the L^2 projection of the exact solution. Then, the following equations are satisfied*

$$(4.7) \quad a(\mathbf{e}_h, \mathbf{v}) - b(\mathbf{v}, \varepsilon_h) = \phi_{\mathbf{u}, p}(\mathbf{v}),$$

$$(4.8) \quad b(\mathbf{e}_h, q) = 0,$$

for all $(\mathbf{v}; q) \in V_h \times W_h$. Here

$$(4.9) \quad \phi_{\mathbf{u}, p}(\mathbf{v}) = l_1(\mathbf{v}, \mathbf{u}) - l_2(\mathbf{v}, p) + s(Q_h \mathbf{u}, \mathbf{v}).$$

Proof. Testing (1.1) by \mathbf{v}_0 with $\mathbf{v} = \{\mathbf{v}_0, \mathbf{v}_b\} \in V_h$ gives

$$(4.10) \quad -(\Delta \mathbf{u}, \mathbf{v}_0) + (\kappa^{-1} \mathbf{u}, \mathbf{v}_0) + (\nabla p, \mathbf{v}_0) = (\mathbf{f}, \mathbf{v}_0).$$

It follows from the integration by parts that

$$-(\Delta \mathbf{u}, \mathbf{v}_0) = \sum_{T \in \mathcal{T}_h} (\nabla \mathbf{u}, \nabla \mathbf{v}_0)_T - \sum_{T \in \mathcal{T}_h} \langle \mathbf{v}_0 - \mathbf{v}_b, \nabla \mathbf{u} \cdot \mathbf{n} \rangle_{\partial T},$$

where we have used the fact that $\sum_{T \in \mathcal{T}_h} \langle \mathbf{v}_b, \nabla \mathbf{u} \cdot \mathbf{n} \rangle_{\partial T} = 0$. Using (4.3) and the equation above, we obtain

$$(4.11) \quad -(\Delta \mathbf{u}, \mathbf{v}_0) = (\nabla_w(Q_h \mathbf{u}), \nabla_w \mathbf{v}) - l_1(\mathbf{v}, \mathbf{u}).$$

Using (4.4), (4.11) and the definition of Q_0 , we have

$$(4.12) \quad \begin{aligned} -(\Delta \mathbf{u}, \mathbf{v}_0) + (\kappa^{-1} \mathbf{u}, \mathbf{v}_0) + (\nabla p, \mathbf{v}_0) &= (\nabla_w(Q_h \mathbf{u}), \nabla_w \mathbf{v}) + (\kappa^{-1} \mathbf{u}, \mathbf{v}_0) \\ &\quad - (\nabla_w \cdot \mathbf{v}, Q_h p) - l_1(\mathbf{v}, \mathbf{u}) + l_2(\mathbf{v}, p) \end{aligned}$$

It follows from (4.10) and (4.12),

$$(\nabla_w(Q_h \mathbf{u}), \nabla_w \mathbf{v}) + (\kappa^{-1} Q_0 \mathbf{u}, \mathbf{v}_0) - (\nabla_w \cdot \mathbf{v}, Q_h p) = (\mathbf{f}, \mathbf{v}_0) + l_1(\mathbf{v}, \mathbf{u}) - l_2(\mathbf{v}, p).$$

Adding $s(Q_h \mathbf{u}, \mathbf{v})$ to the both sides of the equation above gives

$$(4.13) \quad a(Q_h \mathbf{u}, \mathbf{v}) - b(\mathbf{v}, Q_h p) = (\mathbf{f}, \mathbf{v}_0) + \phi_{\mathbf{u}, p}(\mathbf{v}).$$

The difference of (4.13) and (2.7) yields the following equation,

$$(4.14) \quad a(\mathbf{e}_h, \mathbf{v}) - b(\mathbf{v}, \varepsilon_h) = \phi_{\mathbf{u}, p}(\mathbf{v})$$

for all $\mathbf{v} \in V_h$. Next, testing Equation (1.2) by $q \in W_h$ and using (4.2) gives

$$(4.15) \quad (\nabla \cdot \mathbf{u}, q) = (\nabla_w \cdot Q_h \mathbf{u}, q) = 0.$$

The difference of (4.15) and (2.8) yields the following equation.

$$(4.16) \quad b(\mathbf{e}_h, q) = 0, \quad \forall q \in W_h.$$

Combining (4.14) and (4.16) completes the proof of the lemma. \square

5. Preparation for Error Estimates. In this section, we will derive some estimates that can be used in the next section to obtain uniform convergence for velocity and pressure approximations.

The following lemma provides some approximation properties for the projections Q_h , \mathbf{Q}_h and \mathbb{Q}_h . Observe that the underlying mesh \mathcal{T}_h is assumed to be sufficiently general to allow polygons or polyhedra. A proof of the lemma can be found in [14].

LEMMA 5.1. *Let \mathcal{T}_h be a finite element partition of Ω satisfying the shape regularity assumption as specified in [14] and $\mathbf{w} \in [H^{r+1}(\Omega)]^d$ and $\rho \in H^r(\Omega)$ with $1 \leq r \leq k$. Then, for $0 \leq s \leq 1$ we have*

$$(5.1) \quad \sum_{T \in \mathcal{T}_h} h_T^{2s} \|\mathbf{w} - Q_0 \mathbf{w}\|_{T,s}^2 \leq h^{2(r+1)} \|\mathbf{w}\|_{r+1}^2,$$

$$(5.2) \quad \sum_{T \in \mathcal{T}_h} h_T^{2s} \|\nabla \mathbf{w} - \mathbf{Q}_h(\nabla \mathbf{w})\|_{T,s}^2 \leq C h^{2r} \|\mathbf{w}\|_{r+1}^2,$$

$$(5.3) \quad \sum_{T \in \mathcal{T}_h} h_T^{2s} \|\rho - \mathbb{Q}_h \rho\|_{T,s}^2 \leq C h^{2r} \|\rho\|_r^2.$$

Here C denotes a generic constant independent of the meshsize h and the functions in the estimates.

Let T be an element with e as a face. For any function $g \in H^1(T)$, the following trace inequality has been proved to be valid for general meshes described in [14],

$$(5.4) \quad \|g\|_e^2 \leq C (h_T^{-1} \|g\|_T^2 + h_T \|\nabla g\|_T^2).$$

For any finite element function $\mathbf{v} \in V_h$, we introduce the following semi-norm:

$$(5.5) \quad |v|_h = \left(\sum_{T \in \mathcal{T}_h} h_T^{-1} \|\mathbf{v}_0 - \mathbf{v}_b\|_{\partial T}^2 \right)^{1/2}.$$

LEMMA 5.2. Let $r \in [1, k]$. Assume that $\mathbf{w} \in [H^{r+1}(\Omega)]^d$ and $\rho \in H^r(\Omega)$. Then for any $\mathbf{v} \in V_h$ we have

$$(5.6) \quad |s(Q_h \mathbf{w}, \mathbf{v})| \leq Ch^r \|\mathbf{w}\|_{r+1} |\mathbf{v}|_h,$$

$$(5.7) \quad |l_1(\mathbf{v}, \mathbf{w})| \leq Ch^r \|\mathbf{w}\|_{r+1} |\mathbf{v}|_h,$$

$$(5.8) \quad |l_2(\mathbf{v}, \rho)| \leq Ch^r \|\rho\|_r |\mathbf{v}|_h,$$

where $l_1(\cdot, \cdot)$ and $l_2(\cdot, \cdot)$ are defined in (4.5) and (4.6). Thus, the following estimate holds true

$$(5.9) \quad |\phi_{\mathbf{w}, \rho}(\mathbf{v})| \leq Ch^r (\|\mathbf{w}\|_{r+1} + \|\rho\|_r) |\mathbf{v}|_h.$$

Proof. Using the definition of Q_b , (5.4) and (5.1), we have

$$\begin{aligned} |s(Q_h \mathbf{w}, \mathbf{v})| &= \left| \sum_{T \in \mathcal{T}_h} h_T^{-1} \langle Q_0 \mathbf{w} - Q_b \mathbf{w}, \mathbf{v}_0 - \mathbf{v}_b \rangle_{\partial T} \right| \\ &= \left| \sum_{T \in \mathcal{T}_h} h_T^{-1} \langle Q_0 \mathbf{w} - \mathbf{w}, \mathbf{v}_0 - \mathbf{v}_b \rangle_{\partial T} \right| \\ &\leq \left(\sum_{T \in \mathcal{T}_h} (h_T^{-2} \|Q_0 \mathbf{w} - \mathbf{w}\|_T^2 + \|\nabla(Q_0 \mathbf{w} - \mathbf{w})\|_T^2) \right)^{1/2} |\mathbf{v}|_h \\ &\leq Ch^r \|\mathbf{w}\|_{r+1} |\mathbf{v}|_h. \end{aligned}$$

Similarly, it follows from (5.4) and (5.2)

$$\begin{aligned} |l_1(\mathbf{v}, \mathbf{w})| &\equiv \left| \sum_{T \in \mathcal{T}_h} \langle \mathbf{v}_0 - \mathbf{v}_b, \nabla \mathbf{w} \cdot \mathbf{n} - \mathbf{Q}_h(\nabla \mathbf{w}) \cdot \mathbf{n} \rangle_{\partial T} \right| \\ &\leq \left(\sum_{T \in \mathcal{T}_h} h \|\nabla \mathbf{w} \cdot \mathbf{n} - \mathbf{Q}_h(\nabla \mathbf{w}) \cdot \mathbf{n}\|_{\partial T}^2 \right)^{1/2} |\mathbf{v}|_h \\ &\leq Ch^r \|\mathbf{w}\|_{r+1} |\mathbf{v}|_h. \end{aligned}$$

Using (5.4) and (5.3), we have

$$\begin{aligned} |l_2(\mathbf{v}, \rho)| &\equiv \left| \sum_{T \in \mathcal{T}_h} \langle \mathbf{v}_0 - \mathbf{v}_b, (\rho - \mathbb{Q}_h \rho) \mathbf{n} \rangle_{\partial T} \right| \\ &\leq \left(\sum_{T \in \mathcal{T}_h} h_T \|\rho - \mathbb{Q}_h \rho\|_{\partial T}^2 \right)^{1/2} |\mathbf{v}|_h \\ &\leq Ch^r \|\rho\|_r |\mathbf{v}|_h. \end{aligned}$$

This completes the proof of the lemma. \square

6. Error Estimates. The goal of this section is to establish some error estimates for the approximate velocity \mathbf{u}_h in the triple-bar norm and for the approximate pressure p_h in the usual L^2 norm. Our main result can be stated as follows.

THEOREM 6.1. *Let $(\mathbf{u}; p) \in [H_0^1(\Omega) \cap H^{k+1}(\Omega)]^d \times (L_0^2(\Omega) \cap H^k(\Omega))$ with $k \geq 1$ and $(\mathbf{u}_h; p_h) \in V_h \times W_h$ be the solutions of (1.1)-(1.3) and (2.7)-(2.8) respectively. Then, there exists a constant C independent of the meshsize h and the spectral radius of κ such that*

$$(6.1) \quad \|\mathbf{u} - \mathbf{u}_h\| + h|p - p_h|_{1,h} \leq Ch^k(\|\mathbf{u}\|_{k+1} + \|p\|_k).$$

In particular, we have the following weighted- L^2 error estimate:

$$(6.2) \quad \|\kappa^{-\frac{1}{2}}(\mathbf{u} - \mathbf{u}_h)\| \leq Ch^k(\|\mathbf{u}\|_{k+1} + \|p\|_k).$$

Proof. Letting $\mathbf{v} = \mathbf{e}_h$ in (4.7) and $q = \varepsilon_h$ in (4.8) and adding the two resulting equations, we obtain

$$(6.3) \quad \|\mathbf{e}_h\|^2 = \phi_{\mathbf{u},p}(\mathbf{e}_h).$$

Using the estimate (5.9) with $r = k$, $\mathbf{w} = \mathbf{u}$, and $\rho = p$ we arrive at

$$(6.4) \quad \|\mathbf{e}_h\|^2 \leq Ch^k(\|\mathbf{u}\|_{k+1} + \|p\|_k)|\mathbf{e}_h|_h.$$

It is trivial to see that

$$|\mathbf{e}_h|_h \leq C\|\mathbf{e}_h\|.$$

Substituting the above estimate into (6.4) yields the desired error estimate for \mathbf{u}_h .

To derive an estimate for ε_h , we have from (4.7) that

$$(6.5) \quad b(\mathbf{v}, \varepsilon_h) = a(\mathbf{e}_h, \mathbf{v}) - \phi_{\mathbf{u},p}(\mathbf{v}),$$

for all $\mathbf{v} \in V_h$. In particular, by letting $\mathbf{v} = F(\varepsilon_h)$ be the artificial flux of ε_h , we have from Lemma 3.2 that

$$\begin{aligned} |\varepsilon_h|_{1,h}^2 &= b(F(\varepsilon_h), \varepsilon_h) \\ &= a(\mathbf{e}_h, F(\varepsilon_h)) - \phi_{\mathbf{u},p}(F(\varepsilon_h)). \end{aligned}$$

Thus, from the definition of $a(\cdot, \cdot)$ and $F(\varepsilon_h)$ we have

$$\begin{aligned} |\varepsilon_h|_{1,h}^2 &\leq \|\mathbf{e}_h\|_{1,h} \|F(\varepsilon_h)\|_{1,h} + |(\kappa^{-1}\mathbf{e}_0, \kappa\nabla\varepsilon_h)| + Ch^k(\|\mathbf{u}\|_{k+1} + \|p\|_k)|F(\varepsilon_h)|_h \\ &\leq \|\mathbf{e}_h\|_{1,h} \|F(\varepsilon_h)\|_{1,h} + |(\kappa^{-\frac{1}{2}}\mathbf{e}_0, \kappa^{\frac{1}{2}}\nabla\varepsilon_h)| + Ch^k(\|\mathbf{u}\|_{k+1} + \|p\|_k)\|F(\varepsilon_h)\|_{1,h} \\ &\leq Ch^k(\|\mathbf{u}\|_{k+1} + \|p\|_k)\|F(\varepsilon_h)\|_{1,h} + \|\kappa^{-\frac{1}{2}}\mathbf{e}_0\| \|\kappa^{\frac{1}{2}}\nabla\varepsilon_h\| \\ &\leq Ch^k(\|\mathbf{u}\|_{k+1} + \|p\|_k)h^{-1}|\varepsilon_h|_{1,h} + \|\kappa^{-\frac{1}{2}}\mathbf{e}_0\| |\varepsilon_h|_{1,h}. \end{aligned}$$

Dividing $h^{-1}|\varepsilon_h|_{1,h}$ from both sides of the above inequality leads to

$$h|\varepsilon_h|_{1,h} \leq Ch^k(\|\mathbf{u}\|_{k+1} + \|p\|_k) + Ch\|\kappa^{-\frac{1}{2}}\mathbf{e}_0\|.$$

This completes the proof of (6.1). \square

The rest of this section is devoted to an error estimate for the velocity approximation in the standard L^2 norm by following the routine duality argument. The analysis

is very much along the same line as for the Stokes equation [15]. More precisely, let us consider the dual problem which seeks $(\psi; \xi)$ satisfying

$$(6.6) \quad -\Delta\psi + \kappa^{-1}\psi + \nabla\xi = \mathbf{e}_0 \quad \text{in } \Omega,$$

$$(6.7) \quad \nabla \cdot \psi = 0 \quad \text{in } \Omega,$$

$$(6.8) \quad \psi = 0 \quad \text{on } \partial\Omega.$$

Assume that the dual problem has the $[H^2(\Omega)]^d \times H^1(\Omega)$ -regularity property in the sense that the solution $(\psi; \xi) \in [H^2(\Omega)]^d \times H^1(\Omega)$ and the following a priori estimate holds true:

$$(6.9) \quad \|\psi\|_2 + \|\xi\|_1 \leq C\|\mathbf{e}_0\|.$$

The assumption (6.9) is known to be valid when the domain Ω is convex and the permeability tensor κ is not highly varying.

THEOREM 6.2. *Let $(\mathbf{u}; p) \in [H_0^1(\Omega) \cap H^{k+1}(\Omega)]^d \times L_0^2(\Omega) \cap H^k(\Omega)$ with $k \geq 1$ and $(\mathbf{u}_h; p_h) \in V_h \times W_h$ be the solutions of (1.1)-(1.3) and (2.7)-(2.8) respectively. Assume that (6.9) holds true. Then one has the following estimate*

$$(6.10) \quad \|\mathbf{u} - \mathbf{u}_0\| \leq Ch^{k+1}(\|\mathbf{u}\|_{k+1} + \|p\|_k).$$

Proof. Testing (6.6) by \mathbf{e}_0 gives

$$\|Q_0\mathbf{u} - \mathbf{u}_0\|^2 = (\mathbf{e}_0, \mathbf{e}_0) = -(\Delta\psi, \mathbf{e}_0) + (\kappa^{-1}\psi, \mathbf{e}_0) + (\nabla\xi, \mathbf{e}_0).$$

Using (4.12) with $\mathbf{u} = \psi$, $\mathbf{v}_0 = \mathbf{e}_0$ and $p = \xi$, the above equation becomes

$$\begin{aligned} \|Q_0\mathbf{u} - \mathbf{u}_0\|^2 &= (\nabla_w Q_h\psi, \nabla_w \mathbf{e}_h) + (\psi, \kappa^{-1}\mathbf{e}_0) - (\nabla_w \cdot \mathbf{e}_h, Q_h\xi) \\ &\quad - l_1(\mathbf{e}_h, \psi) + l_2(\mathbf{e}_h, \xi) \\ &= (\nabla_w Q_h\psi, \nabla_w \mathbf{e}_h) + (Q_0\psi, \kappa^{-1}\mathbf{e}_0) - (\nabla_w \cdot \mathbf{e}_h, Q_h\xi) \\ &\quad - l_1(\mathbf{e}_h, \psi) + l_2(\mathbf{e}_h, \xi). \end{aligned}$$

Adding and subtracting $s(Q_h\psi, \mathbf{e}_h)$ in the equation above yields

$$\|Q_0\mathbf{u} - \mathbf{u}_0\|^2 = a(Q_h\psi, \mathbf{e}_h) - b(\mathbf{e}_h, Q_h\xi) - \phi_{\psi, \xi}(\mathbf{e}_h),$$

where the functional $\phi_{\psi, \xi}$ is given as in (4.9). Now using the fact that $b(\mathbf{e}_h, Q_h\xi) = 0$ and $b(Q_h\psi, \varepsilon_h) = 0$ we obtain

$$\|Q_0\mathbf{u} - \mathbf{u}_0\|^2 = a(\mathbf{e}_h, Q_h\psi) - b(Q_h\psi, \varepsilon_h) - \phi_{\psi, \xi}(\mathbf{e}_h).$$

Using the first error equation (4.7), we can rewrite the above equation as follows

$$(6.11) \quad \|Q_0\mathbf{u} - \mathbf{u}_0\|^2 = \phi_{\mathbf{u}, p}(Q_h\psi) - \phi_{\psi, \xi}(\mathbf{e}_h).$$

The right-hand side of (6.11) can be bounded by using the estimate (5.9). To this end, using (5.9) with $r = k$, $\mathbf{w} = \mathbf{u}$, and $\rho = p$ we obtain

$$(6.12) \quad |\phi_{\mathbf{u}, p}(Q_h\psi)| \leq Ch^k(\|\mathbf{u}\|_{k+1} + \|p\|_k) |Q_h\psi|_h.$$

Note that from the trace inequality (5.4) and the definition of Q_b we have

$$\begin{aligned} |Q_h \psi|_h^2 &= \sum_{T \in \mathcal{T}_h} h_T^{-1} \|Q_0 \psi - Q_b \psi\|_{\partial T}^2 \\ &\leq \sum_{T \in \mathcal{T}_h} h_T^{-1} \|Q_0 \psi - \psi\|_{\partial T}^2 + \sum_{T \in \mathcal{T}_h} h_T^{-1} \|\psi - Q_b \psi\|_{\partial T}^2 \\ &\leq C \sum_{T \in \mathcal{T}_h} h_T^{-1} \|Q_0 \psi - \psi\|_{\partial T}^2 \leq Ch^2 \|\psi\|_2^2. \end{aligned}$$

Substituting the above into (6.12) gives

$$(6.13) \quad |\phi_{\mathbf{u}, p}(Q_h \psi)| \leq Ch^{k+1} (\|\mathbf{u}\|_{k+1} + \|p\|_k) \|\psi\|_2.$$

Next, using (5.9) with $r = 1$, $\mathbf{w} = \psi$, and $\rho = \xi$ we obtain

$$(6.14) \quad \begin{aligned} |\phi_{\psi, \xi}(\mathbf{e}_h)| &\leq Ch(\|\psi\|_2 + \|\xi\|_1) \|\mathbf{e}_h\|_h \\ &\leq Ch(\|\psi\|_2 + \|\xi\|_1) \|\mathbf{e}_h\|. \end{aligned}$$

Substituting (6.13) and (6.14) into (6.11) yields

$$\|Q_0 \mathbf{u} - \mathbf{u}_0\|^2 \leq Ch^{k+1} (\|\mathbf{u}\|_{k+1} + \|p\|_k) \|\psi\|_2 + Ch(\|\psi\|_2 + \|\xi\|_1) \|\mathbf{e}_h\|.$$

Finally, we apply the regularity estimate (6.9) to the above estimate to obtain

$$\|Q_0 \mathbf{u} - \mathbf{u}_0\| \leq Ch^{k+1} (\|\mathbf{u}\|_{k+1} + \|p\|_k) + Ch \|\mathbf{e}_h\|,$$

which, together with the error estimate (6.1), completes the proof of the lemma. \square

7. Numerical Experiments. The goal of this section is to numerically demonstrate the efficiency of the WG finite element algorithm (2.7)-(2.8) when the lowest order of element (i.e., $k = 1$) is employed. For simplicity, we consider the Brinkman model (1.1)-(1.3) in two dimensional domains. The error for the WG solution of (2.7)-(2.8) is measured in three norms defined as follows:

$$\|\mathbf{v}\|^2 := \sum_{T \in \mathcal{T}_h} \left(\mu \int_T |\nabla_w \mathbf{v}|^2 dx + \int_T \mu \kappa^{-1} \mathbf{v}_0 \cdot \mathbf{v}_0 dx + \int_{\partial T} h_T^{-1} (\mathbf{v}_0 - \mathbf{v}_b)^2 ds \right).$$

$$\|\mathbf{v}\|^2 := \sum_{T \in \mathcal{T}_h} \int_T |\mathbf{v}_0|^2 dx,$$

$$\|q\|^2 := \sum_{T \in \mathcal{T}_h} \int_T |q|^2 dx.$$

Note that $\|\mathbf{v}\|$ is a discrete H^1 norm, and the other two are the standard L^2 norm in the respective spaces. Here $\nabla_w \mathbf{v} \in [P_0(T)]^{2 \times 2}$ is computed on each element $T \in \mathcal{T}_h$ by the following equation

$$(\nabla_w \mathbf{v}, \tau)_T = -(\mathbf{v}_0, \nabla \cdot \tau)_T + \langle \mathbf{v}_b, \tau \cdot \mathbf{n} \rangle_{\partial T}$$

for all $\tau \in [P_0(T)]^{2 \times 2}$. Since τ is constant on the element T , the above equation can be simplified as

$$(\nabla_w \mathbf{v}, \tau)_T = \langle \mathbf{v}_b, \tau \cdot \mathbf{n} \rangle_{\partial T}, \quad \forall \tau \in [P_0(T)]^{2 \times 2}.$$

For any given $\mathbf{v} = \{\mathbf{v}_0, \mathbf{v}_b\} \in V_h$, the discrete weak divergence $\nabla_w \cdot \mathbf{v} \in P_0(T)$ on each element $T \in \mathcal{T}_h$ is computed by solving the following equation

$$(\nabla_w \cdot \mathbf{v}, q)_T = -(\mathbf{v}_0, \nabla q)_T + \langle \mathbf{v}_b \cdot \mathbf{n}, q \rangle_{\partial T}, \quad \forall q \in P_0(T).$$

Since $q|_T \in P_0(T)$, the above equation can be simplified as

$$(\nabla_w \cdot \mathbf{v}, q)_T = \langle \mathbf{v}_b \cdot \mathbf{n}, q \rangle_{\partial T}, \quad \forall q \in P_0(T).$$

The numerical examples of this section have been considered in [9, 10, 16]. Examples 1, 2 and 3 are presented for studying the reliability of the WG method for problems with high contrast of permeability such that κ^{-1} varies from 1 to 10^6 . In such geometry, large highly permeable media connect vugs surrounded by a rather lowly permeable material. Example 1 has known analytical solution (see [16]). But Examples 2 and 3 do not have analytical solutions to the author's knowledge. The profiles of κ^{-1} for examples 2 and 3 can be found in [9].

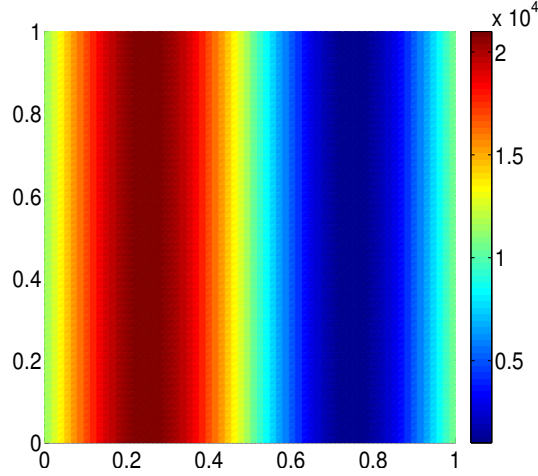


FIG. 7.1. Geometry for κ^{-1} in Example 1 with $a = 10^4$.

7.1. Example 1. This example will test the accuracy and reliability of the method for a giving analytical solutions and highly varying permeability κ . The profile of κ^{-1} is shown in Figure 7.1. Let $\Omega = (0, 1) \times (0, 1)$. The exact solution is given by

$$\mathbf{u} = \begin{pmatrix} \sin(2\pi x) \cos(2\pi y) \\ -\cos(2\pi x) \sin(2\pi y) \end{pmatrix} \text{ and } p = x^2 y^2 - 1/9.$$

It is easy to check that $\nabla \cdot \mathbf{u} = 0$ and $\int_{\Omega} p = 0$. We consider the following permeability

$$\kappa^{-1} = a(\sin(2\pi x) + 1.1),$$

where a is a given constant. The values of κ^{-1} are plotted in Figure 7.1 for $a = 10^4$.

The optimal convergence rates for the corresponding WG solutions are presented in Table 7.1-7.4 for $\mu = 1, 0.01$, and $a = 10, 10^4$. Our numerical results demonstrate that the WG method is accurate and robust.

TABLE 7.1

Example 1. Error and convergence rate for velocity in norm $\|Q_h \mathbf{u} - \mathbf{u}_h\|$ on triangles.

h	$a = 10, \mu = 1$		$a = 10, \mu = 0.01$		$a = 10^4, \mu = 1$		$a = 10^4, \mu = 0.01$	
	Error	Rate	Error	Rate	Error	Rate	Error	Rate
1/16	3.08e-1		1.55e-1		1.58e-1		1.61e-1	
1/24	2.00e-1	1.06	9.90e-2	1.11	1.04e-1	1.02	1.01e-1	1.16
1/32	1.49e-1	1.03	7.28e-2	1.07	7.90e-2	0.97	7.37e-2	1.10
1/40	1.18e-1	1.02	5.76e-2	1.05	6.33e-2	0.93	5.81e-2	1.06
1/48	9.84e-2	1.01	4.77e-2	1.03	5.28e-2	1.00	4.80e-2	1.05
1/56	8.43e-2	1.01	4.08e-2	1.02	4.50e-2	1.00	4.09e-2	1.03
1/64	7.36e-2	1.01	3.56e-2	1.01	3.94e-2	1.00	3.57e-2	1.03

TABLE 7.2

Example 1. Error and convergence rate for velocity in norm $\|Q_0 \mathbf{u} - \mathbf{u}_0\|$ on triangles.

h	$a = 10, \mu = 1$		$a = 10, \mu = 0.01$		$a = 10^4, \mu = 1$		$a = 10^4, \mu = 0.01$	
	Error	Rate	Error	Rate	Error	Rate	Error	Rate
1/16	5.01e-2		5.45e-2		5.84e-2		1.77e-2	
1/24	2.24e-2	1.98	2.64e-2	1.79	2.58e-2	2.02	7.85e-3	2.01
1/32	1.26e-2	1.99	1.53e-2	1.88	1.46e-2	1.97	4.41e-3	2.00
1/40	8.09e-3	2.00	9.97e-3	1.93	9.36e-3	2.00	2.82e-3	2.00
1/48	5.62e-3	2.00	6.99e-3	1.95	6.49e-3	2.00	1.96e-3	2.00
1/56	4.13e-3	2.00	5.16e-3	1.96	4.78e-3	2.00	1.44e-3	2.00
1/64	3.16e-3	2.00	3.97e-3	1.97	3.65e-3	2.00	1.10e-3	2.00

TABLE 7.3

Example 1. Error and convergence rate for velocity in norm $\|\mathbf{u} - \mathbf{u}_0\|$ on triangles.

h	$a = 10, \mu = 1$		$a = 10, \mu = 0.01$		$a = 10^4, \mu = 1$		$a = 10^4, \mu = 0.01$	
	Error	Rate	Error	Rate	Error	Rate	Error	Rate
1/16	3.12e-2		6.70e-2		5.27e-2		6.48e-3	
1/24	1.39e-2	1.99	3.22e-2	1.80	2.33e-2	2.01	2.98e-3	1.92
1/32	7.86e-3	1.99	1.87e-2	1.89	1.30e-2	2.01	1.69e-3	1.96
1/40	5.04e-3	2.00	1.21e-2	1.93	8.44e-3	1.97	1.09e-3	1.98
1/48	3.50e-3	2.00	8.50e-3	1.95	5.86e-3	2.00	7.56e-4	1.99
1/56	2.57e-3	2.00	6.28e-3	1.97	4.30e-3	2.00	5.56e-4	2.00
1/64	1.97e-3	2.00	4.82e-3	1.98	3.29e-3	2.00	4.26e-4	2.00

The rest of the test problems have the following data setting:

$$(7.1) \quad \Omega = (0, 1) \times (0, 1), \quad \mu = 0.01, \quad \mathbf{f} = 0, \quad \mathbf{g} = \begin{pmatrix} 1 \\ 0 \end{pmatrix}.$$

TABLE 7.4

Example 1. Error and convergence rate for pressure in norm $\|Q_h p - p_h\|$ on triangles.

h	$a = 10, \mu = 1$		$a = 10, \mu = 0.01$		$a = 10^4, \mu = 1$		$a = 10^4, \mu = 0.01$	
	Error	Rate	Error	Rate	Error	Rate	Error	Rate
1/16	1.17e-1		4.60e-2		4.97e-1		5.46e-2	
1/24	7.81e-2	1.01	3.24e-2	0.86	3.30e-1	1.00	3.57e-2	1.05
1/32	5.85e-2	1.00	2.49e-2	0.92	2.47e-1	1.00	2.64e-2	1.05
1/40	4.68e-2	1.00	2.01e-2	0.95	1.98e-1	1.00	2.09e-2	1.04
1/48	3.90e-2	1.00	1.69e-2	0.97	1.66e-1	0.97	1.74e-2	1.03
1/56	3.34e-2	1.00	1.45e-2	0.98	1.42e-1	1.00	1.48e-2	1.02
1/64	2.92e-2	1.00	1.27e-2	0.98	1.24e-1	1.00	1.29e-2	1.02

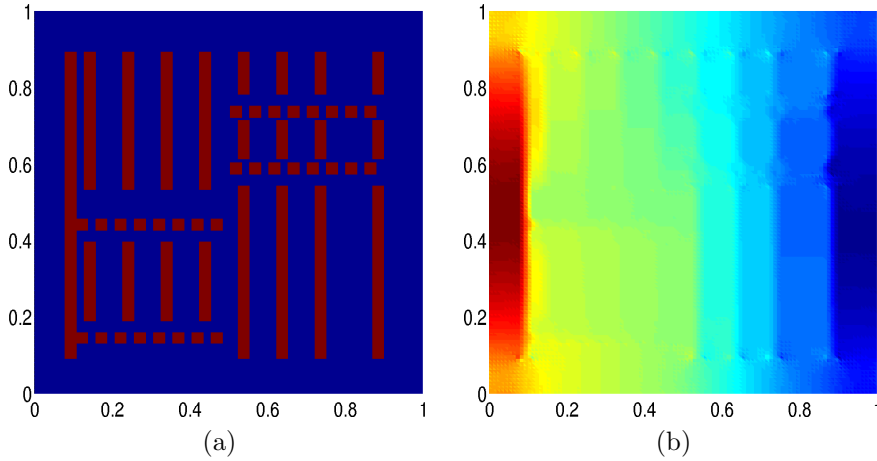


FIG. 7.2. Example 2: (a) Profile of κ^{-1} with low (blue) and high (red); (b) Pressure profile.

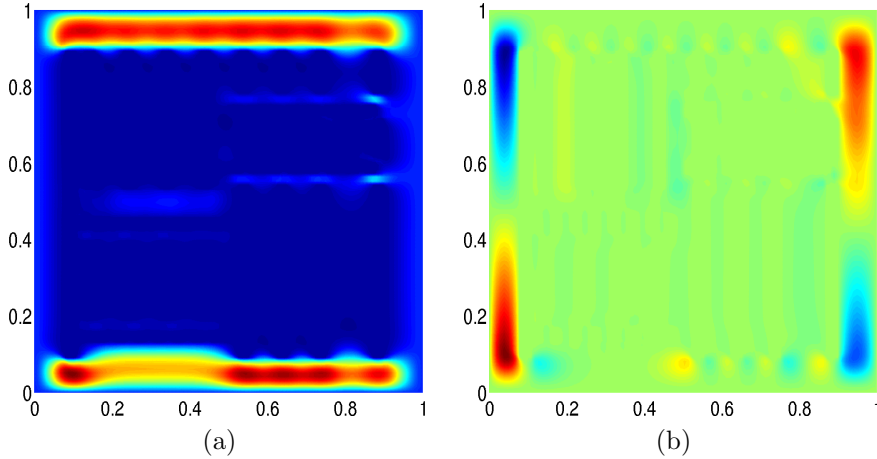


FIG. 7.3. Example 2: (a) First component of velocity u_1 ; (b) Second component of velocity u_2 .

7.2. Example 2. The Brinkman equations (1.1)-(1.3) are solved over a region with a high contrast permeability. The profile of the permeability inverse is plotted

in Figure 7.2 (a) with $\kappa_{\min}^{-1} = 1$ and $\kappa_{\max} = 10^6$ in the red and blue regions.

A 100×100 mesh is used for plotting Figure 7.2 and Figure 7.3. The pressure profile of the WG method is presented in Figure 7.2 (b). The first and the second components of the velocity calculated by the WG method are shown in Figure 7.3(a) and (b) respectively.

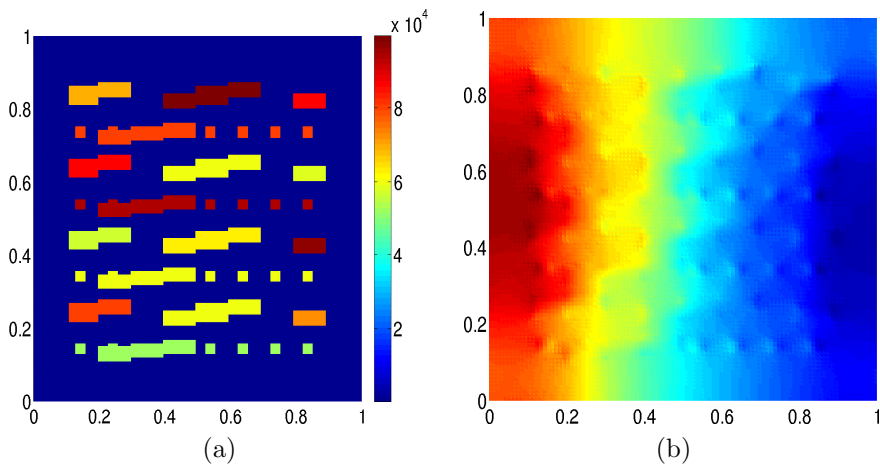


FIG. 7.4. *Example 3: (a) Profile of κ^{-1} ; (b) Pressure profile.*

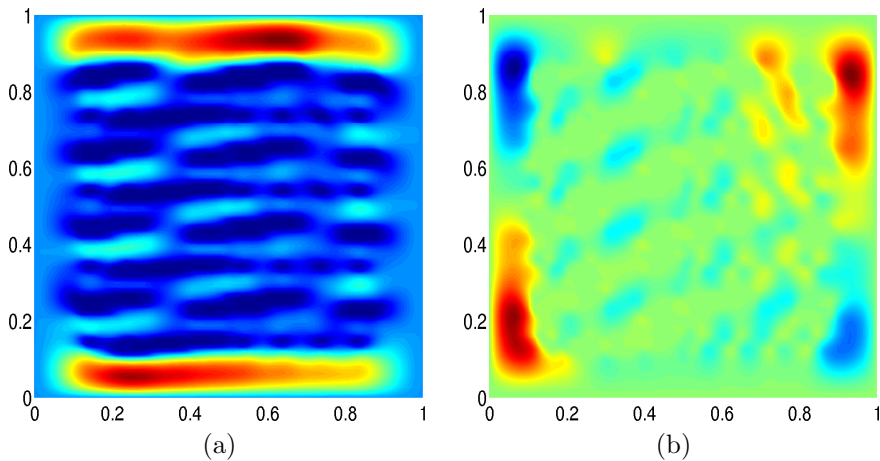


FIG. 7.5. *Example 3: (a) First component of velocity u_1 ; (b) Second component of velocity u_2 .*

7.3. Example 3. This is another example of flow through a region with high contrast permeability. The profile of κ^{-1} is plotted in Figure 7.4(a) and the data for the modeling equation is given in (7.1).

A 100×100 mesh is used for plotting Figure 7.4 and Figure 7.5. The pressure profile of the WG method is presented in Figure 7.4(b). The first and the second components of the velocity calculated by the WG method are shown in Figure 7.5(a) and 7.5(b) respectively.

The rest of the examples simulate flow through porous media with different geometries without known analytical solutions. Flow through vuggy media, fibrous materials and open foam geometries are tested and their permeability inverse profiles can be found in different literatures such as [10, 16].

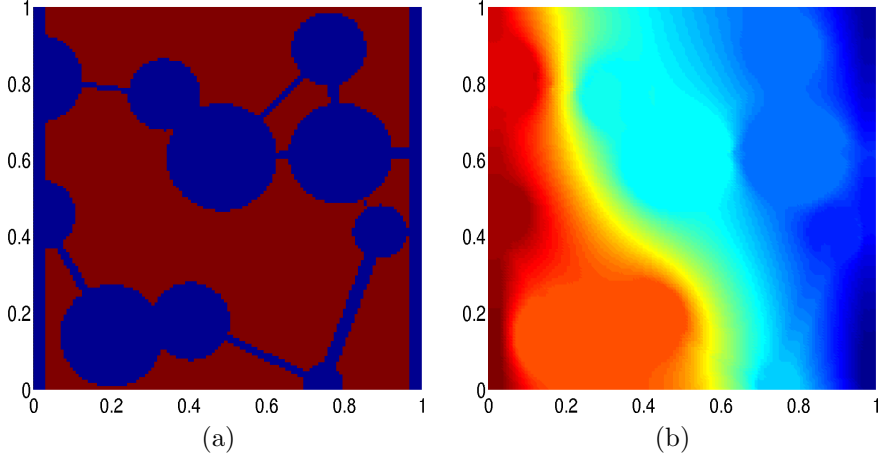


FIG. 7.6. *Example 4: (a) Profile of κ^{-1} for vuggy medium; (b) Pressure profile.*

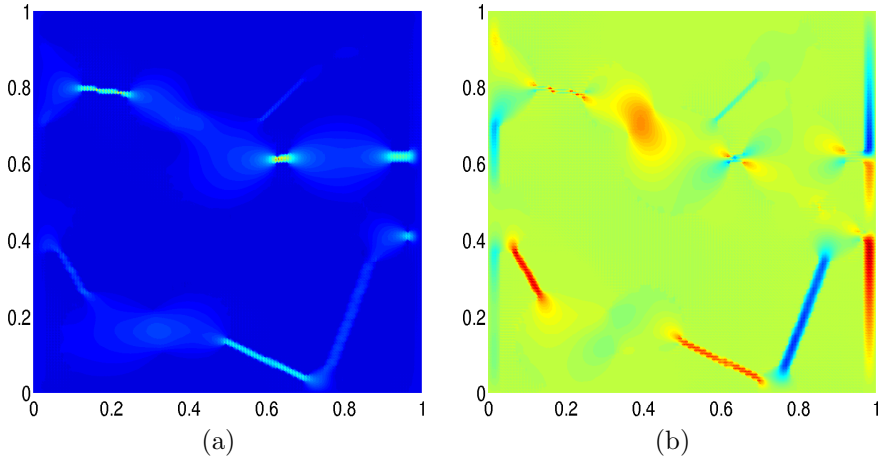


FIG. 7.7. *Example 4: (a) First component of velocity u_1 ; (b) Second component of velocity u_2 .*

7.4. Example 4. In this example, the Brinkman equations (1.1)-(1.3) are solved over a vuggy medium with the data set in (7.1). The profile of κ^{-1} is plotted in Figure 7.6(a).

For this example, a 128×128 mesh is used for plotting Figure 7.6 and Figure 7.7. The pressure profile of the WG method is presented in Figure 7.6(b). The first and the second components of the velocity calculated by the WG method are shown in Figure 7.7(a) and 7.7(b) respectively.

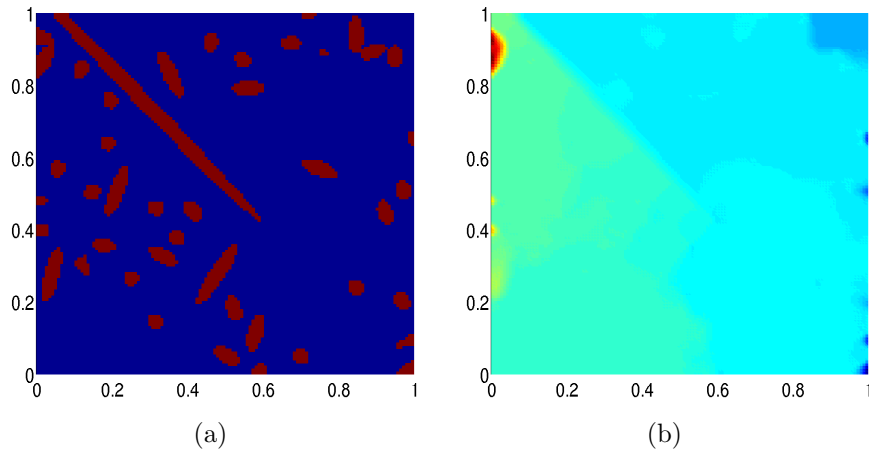


FIG. 7.8. Example 5: (a) Profile of κ^{-1} for fibrous structure; (b) Pressure profile.

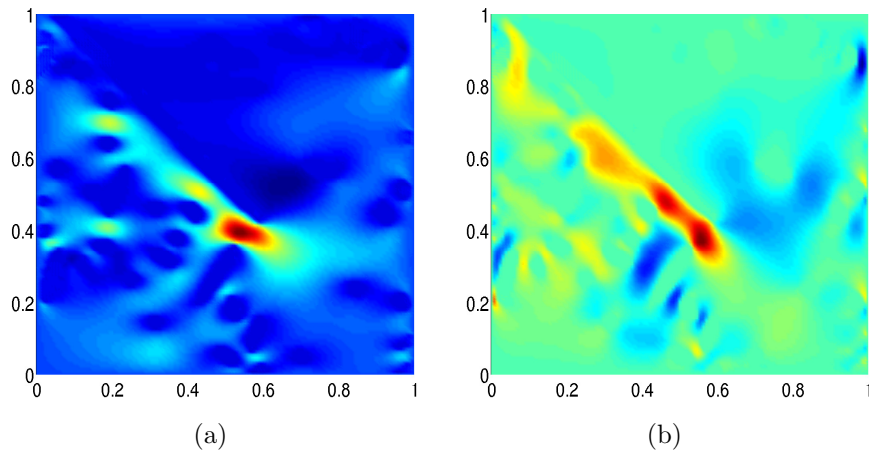


FIG. 7.9. Example 5: (a) First component of velocity u_1 ; (b) Second component of velocity u_2 .

7.5. Example 5. This example is frequently used in filtration and insulation materials. The inverse of permeability of fibrous structure is shown in Figure 7.8(a). A 128×128 mesh is used for plotting Figure 7.8 and Figure 7.9. The pressure profile of the WG method is presented in Figure 7.8(b). The first and the second components of the velocity calculated by the WG method are shown in Figure 7.9(a) and 7.9(b) respectively.

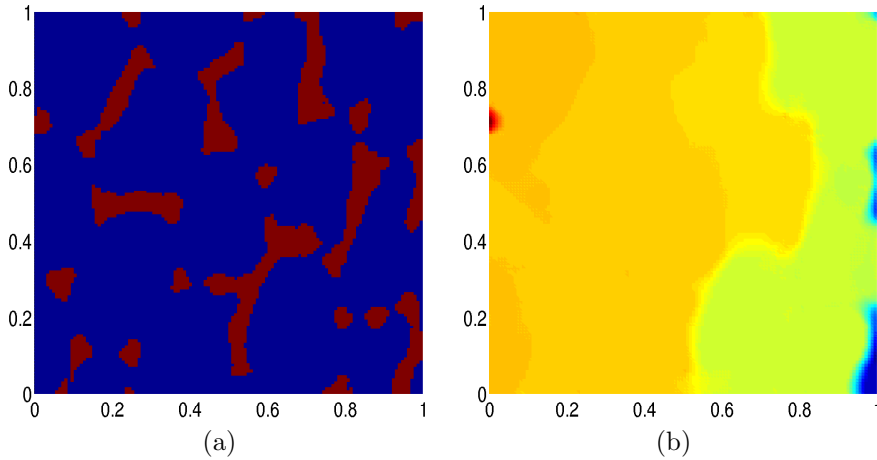


FIG. 7.10. Example 6: (a) Profile of κ^{-1} for open form; (b) Pressure profile.

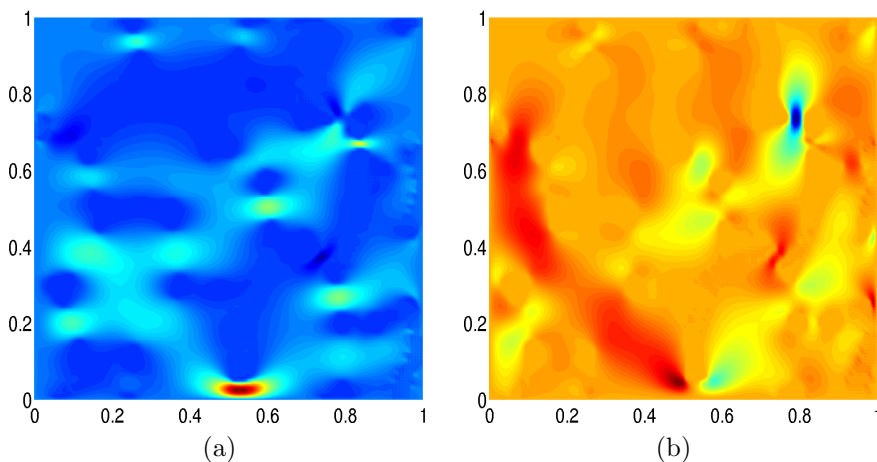


FIG. 7.11. Example 6: (a) First component of velocity u_1 ; (b) Second component of velocity u_2 .

7.6. Example 6. The geometry of this example is an open foam with a profile of κ^{-1} shown in Figure 7.10(a). The rest of the modeling data is given in (7.1). Figure 7.10 and Figure 7.11 are plotted over a 128×128 grid. The profiles of the approximate pressure and velocity are presented in Figure 7.10(b) and Figure 7.11 respectively.

REFERENCES

- [1] S. BADIA AND R. CODINA *Unified stabilized finite element formulations for the Stokes and the Darcy problems*, SIAM J. Numer. Anal., 47 (2009), 1971–2000.
- [2] I. BABUŠKA, *The finite element method with Lagrangian multiplier*, Numer. Math., 20 (1973), 179–192.
- [3] S. BRENNER AND R. SCOTT, *Mathematical theory of finite element methods*, Springer, 2002.
- [4] F. BREZZI, *On the existence, uniqueness, and approximation of saddle point problems arising from Lagrangian multipliers*, RAIRO, Anal. Numér., 2 (1974), 129–151.
- [5] F. BREZZI AND M. FORTIN, *Mixed and Hybrid Finite Elements*, Springer-Verlag, New York, 1991.

- [6] M. CROUZEIX AND P. RAVIART, *Conforming and nonconforming finite element methods for solving the stationary Stokes equations*, RAIRO Anal. Numer., 7 (1973), 33–76.
- [7] V. GIRAULT AND P. RAVIART, *Finite Element Methods for the Navier-Stokes Equations: Theory and Algorithms*, Springer-Verlag, Berlin, 1986.
- [8] M. GUNZBURGER, *Finite Element Methods for Viscous Incompressible Flows, A Guide to Theory, Practice and Algorithms*, Academic, San Diego, 1989.
- [9] Y. EFENDIEV, J. GALVIS, R. LAZAROV, AND J. WILLEMS, *Robust domain decomposition preconditioners for abstract symmetric positive definite bilinear forms*, arXiv:1105.1131.
- [10] O. ILIEV, R. LAZAROV, AND J. WILLEMS, *Variational multiscale finite element method for flows in highly porous media*, Multiscale Modeling & Simulation, 9(4) (2011), 1350–1372.
- [11] J. KNN AND R. STENBERG, *$H(\text{div})$ -conforming finite elements for the Brinkman problem*, Math. Models and Meth. Applied Sciences, 11 (2011), 2227–2248.
- [12] K. MARDAL, X. TAI, AND R. WINTHER *A Robust finite element method for Darcy-Stokes flow*, SIAM J. Numer. Anal., 40 (2002), 1605-1631.
- [13] J. WANG AND X. YE, *A weak Galerkin finite element method for second-order elliptic problems*, J. Comp. and Appl. Math, 241 (2013) 103-115, arXiv:1104.2897v1.
- [14] J. WANG AND X. YE, *A Weak Galerkin mixed finite element method for second-order elliptic problems*, Math. Comp., to appear, arXiv:1202.3655v1.
- [15] J. WANG AND X. YE, *A Weak Galerkin finite element method for the Stokes equations*, arXiv:1302.2707v1.
- [16] J. WILLEMS, *Numerical upscaling for multiscale flow problems*, Ph.D Thesis, 2009.